# *Design Principles for SuCESsFul Biosensors: Specific Fluorophore/Analyte Binding and Minimization of Fluorophore/Scaffold Interactions*



**Citation:** De Picciotto, Seymour et al. "Design Principles for SuCESsFul Biosensors: Specific Fluorophore/Analyte Binding and Minimization of Fluorophore/Scaffold Interactions." Journal of Molecular Biology 428, 20 (October 2016): 4228–4241 © 2016 Elsevier Ltd

**As Published:** http://dx.doi.org/10.1016/J.JMB.2016.07.004

**Publisher:** Elsevier BV

**Persistent URL:** http://hdl.handle.net/1721.1/116522

**Version:** Author's final manuscript: final author's manuscript post peer review, without publisher's formatting or copy editing

HHS Public Access

Author manuscript

*J Mol Biol*. Author manuscript; available in PMC 2017 October 09.

Published in final edited form as:

*J Mol Biol*. 2016 October 9; 428(20): 4228–4241. doi:10.1016/j.jmb.2016.07.004.

# Design principles for reagentless biosensors: specific fluorophore/analyte binding and minimization of fluorophore/scaffold interactions

**Seymour de Picciotto**[1], **Paige M. Dickson**[2], **Michael W. Traxlmayr**[3], **Bryan S. Marques**[4], **Elke Socher**[5], **Sixing Zhao**[1], **Stephanie Cheung**[5], **Jonathan Kiefer**[6], **A. Joshua Wand**[4], **Linda G. Griffith**[1,4], **Barbara Imperiali**[5,7], and **K. Dane Wittrup**[1,3,8,**]

[1]Department of Biological Engineering, Massachusetts Institute of Technology

[2]Department of Chemistry, Northeastern University

[3]Koch Institute for Integrative Cancer Research

[4]Department of Biochemistry & Biophysics, University of Pennsylvania

[5]Department of Chemistry, Massachusetts Institute of Technology

[6]Department of Chemistry and Applied Biosciences, Institute of Pharmaceutical Sciences, Swiss, Federal Institute of Technology, Zurich

[7]Department of Biology, Massachusetts Institute of Technology

[8]Department of Chemical Engineering, Massachusetts Institute of Technology

## Abstract

Quantifying protein location and concentration is critical for understanding function *in situ*. SuCESsFul biosensors, in which a reporting fluorophore is conjugated to a binding scaffold, can in principle detect analytes of interest with high temporal and spatial resolution. However, their adoption has been limited due to the extensive empirical screening required for their development. We sought to establish design principles for this class of biosensor by characterizing over 400 biosensors based on various protein analytes, binding proteins and fluorophores. We found that the brightest readouts are attained when a specific binding pocket for the fluorophore is present on the analyte. Also, interaction of the fluorophore with the binding protein it is conjugated to can raise background fluorescence, considerably limiting sensor dynamic range. Exploiting these two

**Address correspondence to: K. Dane Wittrup, Building 76-261, 500 Main Street, Cambridge, MA 02139, Phone: 617-253-4578, wittrup@MIT.EDU.

**Competing financial interests**

The authors declare no competing financial interests.

**Authors contribution**

S. P. designed and performed experiments, analyzed data, and wrote the manuscript. P. M. D., S. Z., and J. K. performed experiments. M. W. T., E. S., S. C. designed and performed experiments. B.S.M. conducted NMR experiment. A. J. W and B. S. M. analyzed NMR data. L. G. G., B. I. and K. D. W. designed experiments, analyzed data and edited the manuscript.

concepts, we designed biosensors that attain a 100-fold increase in fluorescence upon binding to analyte, an order of magnitude improvement over the previously best reported SuCESsFul biosensor. These design principles should facilitate the development of improved SuCESsFul biosensors.

## Graphical abstract

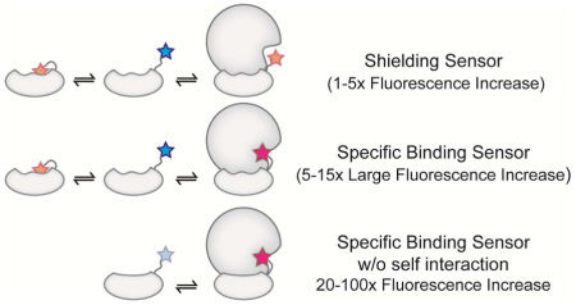


### Keywords

Solvatochromism; Sso7d scaffold; Sensors; Protein engineering; Directed evolution

## Introduction

Spatial and temporal fluctuations in the level of proteins in living systems contain valuable functional information that is difficult to obtain at high resolution in a non-destructive fashion. An ideal sensor would report the concentration and localization of a target analyte in real-time without interfering with its function. Sensors such as those based on Forster Resonance Energy Transfer (FRET) couple the analyte recognition and signal transduction event into a single step and provide temporal and spatial resolution[1]. However, such sensors require the introduction of two unique fluorophores into either two binders or into proteins, which undergo large conformational changes upon binding. In 1964, Burr and Koshland introduced a novel concept in which an environment-sensitive fluorophore is coupled to a single analyte-specific binder[2]. Changes in the environment of the fluorophore (such as solvent shielding) upon analyte binding transduce the binding signal into a fluorescence read-out. Several groups have reported the development and application of this class of biosensors, with the historical label of “reagentless biosensors”[3–8]. Due to the illogic of this previous nomenclature (since the sensor is itself a reagent), in this work we have termed this class of engineered molecules as SuCESsFul (Scaffold Conjugated to Environment Sensitive Fluorophore) biosensors.

Currently, SuCESsFul biosensors are designed in three steps. First, a binder is engineered against the intended target using established display technologies[9–12] and multiple scaffolds[13–15] , ideally with tailored binding kinetics and affinity[16]. The second step is careful choice of the labeling site. Three rules have been established for this process: the residue must be: 1) exposed to solvent, 2) non-perturbing to the analyte/scaffold interaction, and 3) close to the binding epitope. This last step remains challenging as it is somewhat at

odds with the second rule. Finally, a fluorophore is conjugated to a specific site on the binding protein using established chemical[17] or enzymatic[18] techniques. Typically, cysteines are introduced at the desired labeling position via site-directed mutagenesis and conjugated to thiol-reactive fluorophores. Unfortunately, the growth in reports of SuCESsFul biosensors has not been commensurate with their promise, perhaps due to as-yet poorly defined limitations of the design process.

In this work we have designed over 400 SuCESsFul biosensors against various analytes using multiple scaffolds and fluorophores, but found that successful designs with significant dynamic signal range (above two-fold) were quite rare, which is quantitatively consistent with the literature. In this study, we investigated both the analyte-bound and unbound states and assessed the mechanisms accounting for bright fluorescence in the bound state and dim fluorescence in the unbound state. First, from an in-depth characterization of the strongest sensor previously reported (dynamic range 10–15-fold from bound to unbound[4]), we discovered that a specific binding pocket for the fluorophore on the analyte greatly enhanced the fluorescence in the bound state. Second, we found that fluorophores conjugated to locally stable scaffold structures generate lower background signal in the unbound state. Combining these observations, we devised sensors with up to 100-fold dynamic range, the most responsive sensors reported to date for protein analytes. In future studies, application of these two design principles for minimizing unbound fluorescence and maximizing bound fluorescence via specific interactions should facilitate the development of useful sensors to enable the study of dynamic fluctuations of proteins in living cells and tissues.

## Material & Methods

### Fibronectin engineering by yeast surface display

We choose the human 10$^{th}$ Fibronectin 3 domain as a scaffold to engineer binders as it has been a well validated protein engineering scaffold and it is free of cysteines [21,23]. Our group has published a detailed protocol for fibronectin engineering by yeast surface display [20]. Briefly, binders were isolated by magnetic bead sorts from the G4 library [19]. Initial clones were then affinity matured by error-prone polymerase chain reaction (PCR) and selected by fluorescence activated cell sorting (FACS). Biotinylated analyte was detected with either Streptavidin Alexa Fluor 647 (Invitrogen) or Anti-Biotin antibody (eBiosciences) in alternation. For determination of $K_d$ values lead clones were titrated on the surface of yeasts, and data were fitted to a monovalent binding isotherm.

### Protein expression and purification

We found that cysteine containing fibronectins were poorly soluble as opposed to their cysteine-free counterparts. In order to increase yield and solubility, crucial for subsequent fluorophore conjugation, we chose to express fibronectins fused to a N-terminal hexahistidine tag and small ubiquitylation modified (SUMO) tag. Thus, all protein encoding genes were cloned in a pE-sumo expression vector (LifeSensors) by restriction digest using the XbaI and BsaI sites. The sequence confirmed plasmid were transformed into Rosetta 2 (DE3) cells (Millipore) or XL1-Blue (Agilent) and grown overnight in 5mL LB media + Kanamycin (50ug/ml) at 37°C. Subsequently, the cultures were diluted 200-fold in Terrific

Broth + kanamycin. When cells had reached an $OD_{600}$ = 1.0–2.0, expression was induced by addition of 500 μM Isopropyl β-D-1-thiogalactopyranoside IPTG (AMRESCO). After overnight expression at 20°C, cultures were centrifuged and the pellets were resuspended in 50mM Sodium Phosphate (AMRESCO), 300mM Sodium Chloride (AMRESCO), 1% Glycerol (AMRESCO), 3% Triton-X-100 (AMRESCO) at pH 8.0. Cells were sonicated and centrifuged, followed by filter sterilization of the supernatant and purification on a Ni-NTA resin (QIAGEN). Purification fractions were ran on a 4–12% bis-tris acrylamide gel to confirm expression and purity (Life Technologies). The elution fractions were dialyzed into PBS using Snakeskin dialysis tubing (Thermo Scientific), samples were concentrated to >100 μM with an amicon 3K concentrator, flash frozen in liquid nitrogen, and stored at 80°C.

DARPins were either expressed as N-terminal His6-Sumo fusions or as N-terminal His6 only fusions on a pQE vector (gift from the Pluckthun laboratory). Expression and purification methods were the same as described above.

Sso7d proteins were expressed with an N-terminal histidine tag in Rosetta 2 (DE3) cells on a custom pE based vector ($GH_6GG$-Sso7d). Proteins were purified under denaturing conditions in the presence of 2mM β-mercaptoethanol. Following labeling, the proteins were purified by cation exchange in 20mM Tris pH 8.0 with a gradient from 0 to 1 M NaCl on a SP FF column (GE Healthcare).

All Maltose Binding Protein mutants were expressed with an N-terminal His6 tag (pQE vector, gift from Pluckthun laboratory). Abl-SH2 and Src-SH3 were also cloned into the pE-sumo expression vector, expressed and purified like other sumo fusion proteins in this study. Chicken egg lysozyme was purchased from Sigma and dissolved in PBS. For yeast surface display screenings, we purchased Amphiregulin, Betacellulin, Epidermal Growth Factor and Epiregulin from Peprotech. For further characterization and fluorescence assays, BTC and EGF were expressed as His6-Sumo N-terminal fusion as described previously[47]. Fatty acid free mouse serum albumin was purchased from Alpha Diagnostic International.

## Protein Labeling

For labeling, the protein sample was diluted to a final concentration of 100 μM in PBS and the reducing agent (tris(2-carboxyethyl)phosphine (TCEP) was added to a final concentration of 1 mM. After 60 minute incubation at room temperature for thiol reduction, the thiol reactive fluorophore was added to a final concentration of 1mM and the sample was reacted overnight on a rotating wheel at room temperature. Free fluorophore was removed on a G-25 desalting resin (GE Healthcare). Labeling efficiencies were in the range of 0.4–0.8 fluorophore/protein molar ratio, as derived from the A280 and fluorophore absorbance[4]. NBD, IAEDANS, MIANS, Badan were purchased (Life Technologies), 4-DMN and 4-DMAP were synthesized (see below).

## Fluorophore synthesis

The 4-DMAP-cysteine labeling agent was synthesized with a short linker (3A) following published procedures for 4-DMN[45] starting with the 4-DMAP anhydride precursor[48]. The

purification was improved by using a chloroform/methanol (0–5%) solvent system and adding 0.2% acetic acid. The product was a bright yellow solid.

### Protein biotinylation

Samples were biotinylated with Sulfo-NHS-LC-Biotin (Thermo) in PBS for 1h at room temperature and quenched with Tris buffer at pH 8.0. Excess biotin was removed on a zeba spin 7k desalting column. Extent of biotinylation was confirmed by MALDI-TOF mass spectrometry.

### Size exclusion chromatography

All size exclusion chromatography was performed on an AKTA system (GE Healthcare). Analytical runs were performed in PBS at pH 7.4 on a Superdex 75 10/300 GL column at 0.75mL/min. Preparative runs were performed in PBS on a Superdex 75 16/60 column at 1mL/min.

### Fluorescence Measurements

Spectroscopy studies were performed using a FluoroMax-2 Fluorometer with an integration time of 0.100 s, excitation and emission slits set at 5 and 10 nm respectively. All excitation wavelengths and emission scans are listed in Supplementary Table 1. Stern Volmer constants from the iodide quencing experiment were extract from titration with 0–200 mM potassium iodide as described previously[49].

### Biolayer Interferometry

Experiments were performed on a Blitz or an Octet RED instrument (ForteBio) in PBS, 1mg/ml bovine serum albumin, 0.002% v/v Tween-20.

### YSD for enhanced MBP mutant isolation

The gene for Maltose Binding Protein was cloned between the NheI and BamHI restriction sites in the pCTcon2 vector for display as an N-terminal fusion to Aga2p. To generate the MBP 1.0 library, mutations were introduced in the MBP gene as described for fibronectin domains[20]. For the cavity targeted libraries, regions covering amino acids 150–158 and 344–352 were amplified with primers allowing yeast homologous recombination. The error prone PCR condition were similar to those of fibronectin loops[20]. The other fragments were amplified without error-prone PCR. The gene fragments were combined and transformed into EBY100 yeasts, allowing the yeasts to perform homologous recombination. Two NBD conjugated Off7 mutants (T46C and M114C) were added at 1uM to each library independently and sorted by flow cytometry. The fluorescence of NBD was detected under the FITC channel. Two rounds of sorting were performed to obtain a clean polyclonal population.

### Sequence analysis

177 sequences were obtained by sanger sequencing. MiSeq yielded 8.4 million past filter reads (see Supplementary table 2). All sequences from the MBP display screen were

analyzed by a user-developed MatLab script, allowing the extraction of several parameters such as amino acid frequency. This code is available upon request.

## NMR Spectroscopy

**Protein Expression/Purification and Sample Preparations—**Maltose binding protein (MBP) from *E. Coli* was expressed in BL21(DE3) *E. coli* during growth on M9 minimal media in 99% $D_2O$ containing $^{15}NH_4Cl$ and $^{13}C_6$-d-glucose as the only sources of nitrogen and carbon, respectively[50]. The MBP was purified as previously described[50,51] with no β-cyclodextrin in any buffers. All isotopically labeled chemicals were obtained from Cambridge Isotopes Laboratories (Andover, MA). Off7 and Off7(T46C)*NBD were purified as described above, and were additionally purified by size exclusion chromatography on a HiLoad 16/60 Superdex 75 column (GE Healthcare). Complexes of MBP and Off7 variants were prepared in 20 mM sodium phosphate, pH 7.5, with 5 mM EDTA by titration of a concentrated solution of Off7 into a ~0.8 mM solution of MBP to a molar ratio of MBP:Off7 = 1:1.2.

**NMR Spectroscopy—**All NMR experiments were collected at 37°C on a 750 MHz ($^1$H) Bruker AVANCE III spectrometer equipped with a TXI cryoprobe. The binding of Off7 variants to MBP was followed using conventionally sampled $^{15}$N-TROSY spectra obtained at 750 MHz ($^1$H) with 16 scans per free induction decay, 128 complex increments in nitrogen and a 1.8 s recycle delay. Backbone resonance assignments of complexed MBP were obtained from non-uniformly sampled[52,53] versions of TROSY-enhanced HNCA [54,55] and HN(CO)CA [55] spectra collected with 10% Poisson-gap sampling, 16 scans per free induction decay, 60 complex increments in nitrogen, 80 complex increments in carbon, and a 1.8 s recycle delay. Data were processed with Felix (Accelrys) and NMRPipe [56].

**Data Analysis—**Backbone resonance assignments of MBP in the various complexes were manually obtained using Sparky[57]. The weighted chemical shift perturbation (CSP) is expressed as:

$$CSP = \sqrt{(\Delta\delta_H)^2 + \left|\frac{\gamma_N}{\gamma_H}\right|(\Delta\delta_N)^2}$$

Where $\Delta\delta_H$ and $\Delta\delta_H$ are the changes in amide hydrogen and nitrogen chemical shifts upon complexation and $\gamma_N$ and $\gamma_H$ are the gyromagnetic ratios of $^{15}$N and $^1$H, respectively. The CSP for each residue was then mapped to the molecular surface of MBP using PyMOL[58].

## Flow cytometry

Samples were analyzed on an Accuri C6 cytometer (Becton Dickinson, BD), 96-well plates were run on a FACSCalibur HTS with a high throughput plate sampler (BD), and sorting was performed on a MoFlo instrument (Beckman Coulter) or a FACSAria instrument (BD). Protein display was detected using anti epitope tag antibodies, either mouse anti HA (clone 16B12, Covance), chicken anti c-myc (Gallus Immunotech) or mouse anti c-myc (clone 9E10, Covance). Secondary labeling was performed using goat anti mouse or chicken

antibody conjugated to AlexaFluor488 or 647 (Life Technologies). Biotinylated analytes were detected with Streptavidin Alexa Fluor 647 or 488 (Life technologies) or anti-biotin-PE antibody (eBiosciences).

### EGF epitope mapping

To identify the binding epitope of Fibronectin clone EGF-A, we chose an epitope mapping approach. Human EGF was fused to Aga2p with a $(G_4S)_3$ linker. Of the 53 amino acids in the protein, we mutated all 36 solvent exposed, non cysteine, proline or glycine residues to an amino acid with opposite side chain properties[59]. Binding of biotinylated fibronectin EGF-A to yeast displayed EGF-mutants was tested at 10 nM and detected with Streptavidin Alexa 647.

## Results

### Successfully designed SuCESsFul biosensors are rare

We evaluated the dynamic signaling range of 426 different binder/fluorophore/analyte combinations to establish the underlying distribution of performance for this class of SuCESsFul biosensors. We generated numerous novel binders based on the 10$^{th}$ type 3 domain of human fibronectin (Fn3)[19], and also reproduced published results for several previously described SuCESsFul biosensors, including the Designed Ankyrin Repeat Protein (DARPin) clone Off7 against maltose binding protein (MBP)[4] from *E. Coli*. To obtain Fn3-based binders, the G4 yeast library was selected against biotinylated Betacellulin (BTC) and Epidermal Growth Factor (EGF) following standard procedures[20]. The lead binders showed single-digit nM dissociation constants (supplementary Fig. S1A–C), and the EGF binder was specific (Supplementary Fig. S1D) and competitive with EGFR binding (Supplementary Fig. S2). In addition, based on literature precedent, we investigated four additional Fn3s, each recognizing MBP[21], the Src SH3 domain[5], the Abl SH2 domain[22], and Hen Egg Lysozyme[23] (Fig 1A). Next, we selected conjugation sites for various solvatochromic fluorophores, which had been applied previously in SuCESsFul biosensors: Nitrobenz-2-Oxa-1,3-Diazole (NBD), 6-Bromoacetyl-2-Dimethylaminonaphthalene (Badan), 1,5-IAEDANS, 5-((((2-Iodoacetyl)amino)ethyl)amino)Naphthalene-1-Sulfonic Acid (IAEDANS), 2-(4-maleimidylanilino)naphthalene-6-sulfonic acid (MIANS), 4-N,N-dimethylamino-1,8-naphthalimide (4-DMN-1,2,3,4 and 5), and 4-dimethylaminophthalimide (4-DMAP) (Supplementary Table S4 and Fig. S3) on each of these scaffolds. The choice of fluorophore conjugation site was intended to position the solvatochromatic fluorophore at the periphery of the interface without interfering with binding. Finally, the purified constructs were tested for their fluorescence properties with and without the target analyte (Fig. 1B). SuCESsFul biosensors are evaluated based on the fold-change in fluorescence between the background ($F_0$) and bound state (F), where $F/F_0$ ratios much greater than one are desired. Overall, the frequency of sensors showing a change in signal ($F/F_0$) greater than two-fold was only 4.0% (17 out of 426, Fig. 1C). Our results are quantitatively consistent with the success rate found in literature (Fig. 1C). Overall, these results clearly demonstrate that the current state-of-the-art approach only rarely generates SuCESsFul biosensors with a dynamic signaling range over twofold.

## A specific binding pocket for NBD is responsible for strong fluorescence activation in an exemplary strong sensor

Given the disappointing results summarized in Fig. 1C, we undertook detailed structure/function analysis of a previously reported successful biosensor in an attempt to elucidate the underlying molecular mechanism that differentiates a successful example from the great majority of marginally useful constructs. We turned our attention to the NBD-labeled DARPin Off7 recognizing MBP, which has been demonstrated to exhibit a 15-fold difference in fluorescence upon MBP-binding [4]. To our knowledge, this represents the biosensor with the largest $F/F_0$ ratio published for a protein/protein interaction to date. We found that the Off7/MBP SuCESsFul biosensor showed fluorescence changes only when conjugated with the fluorophore NBD (Fig. 2A), and not with nine other solvatochromic fluorophores, which belonged to diverse structural classes, suggestive of a specific interaction between NBD and MBP, as opposed to a general nonspecific solvent-shielding mechanism. When labeled at positions N45 or T46, Off7 shows the greatest increase in fluorescence (Fig. 2A), in accordance with previously reported data[4]. Because these two labeling sites are adjacent, we hypothesized the fluorescence activation of NBD might involve a specific interaction with a binding pocket on MBP. To elucidate the nature of this interaction, we examined the crystal structure of the Off7/MBP complex (PDB code: 1SVX) and based on the dimensions of NBD (Supplementary Fig. S4A) we identified 14 amino acids within likely contact distance of NBD when labeled at positions N45 or T46. We noted that there is a small cavity at this site in the wild-type MBP (wtMBP) structure that could potentially serve as a binding site for NBD (Supplementary Fig. S4B). We constructed individual alanine mutants of MBP at each of these positions. All mutants showed similar expression levels and size exclusion chromatography profiles as the wtMBP (Fig. S4C, S4D), indicating structural integrity was maintained. We then measured the fluorescence signal of 300 nM NBD-labeled Off7 in the presence of 10 μM of each of these MBP mutants. We used the M114C sensor (Fig. 2A, M114C*NBD $F/F_0 = 5$) as a control because the fluorophore is on the distal side of MBP; none of the mutations showed any effect on this sensor (Fig. 2D). For the other two labeling sites (N45, T46), we observed changes in the fluorescence intensity (Fig. 2D) and emission wavelength ($\lambda_{maxEm}$) (Supplementary Fig. S4E) compared to wtMBP; the mutations with the greatest reduction of fluorescence activation are found around the cavity in MBP (Fig. 2E). In order to investigate the role of this cavity in more detail, we performed a more detailed analysis of the seven residues (Fig. 2F) forming this pocket by mutating them to smaller and larger side chains. We observed that most mutations in those cavity-forming residues resulted in strongly reduced biosensor activity (Fig. 2G). Fluorescence reductions were most pronounced for mutations to tryptophan. Importantly, the structural integrity (Supplementary Fig. S5A and B) and binding were retained (supplementary Fig. S5C). We hypothesize that when a bulky tryptophan side chain is present at residues 347, 348, or 351, it fills the cavity and sterically interferes with NBD insertion into the cavity. We also identified two mutations, V347F and V347A, which enhanced the activity of the sensor, with the latter yielding a sensor with a remarkable 75-fold increase in fluorescence over background, possibly resulting from improved binding of the fluorophore to the MBP cavity. Together, these data strongly suggest that the Off7-conjugated NBD binds specifically within a hydrophobic cavity in the target analyte MBP, resulting in strong activation of fluorescence.

We next sought to validate the presence of an NBD binding pocket by a library screening strategy. In an inversion of the usual binder maturation process, we matured mutants of the analyte (MBP) for increased fluorescence of the fixed Off7*NBD biosensor (Fig. 3A). We assembled four libraries for yeast surface display, three with mutations focused on the cavity, and one with mutations introduced over the entire gene (supplementary Fig. S6A, S6B). These libraries showed strong protein display on yeast surface and binding to Off7 (supplementary Fig. S6C). The yeast displayed libraries were incubated with 1 μM Off7(T46C)*NBD and sorted by flow cytometry for NBD fluorescence (Fig. 3B). After two rounds of selections, we analyzed the libraries by deep sequencing. The majority of mutations were within the hypothesized NBD binding pocket (Fig. 3C, D, S6D, E). However, multiple mutations were also enriched in the maltose-binding pocket (Fig. 3D, S6D, E). From this we selected the six most frequently observed mutations (three around the NBD cavity, three around the maltose pocket) and expressed the single point mutants as soluble proteins (Supplementary Fig. S6F). All mutations enhanced fluorescence activation on their own (Fig. 3E). Having observed several mutations near the maltose-binding pocket, we investigated whether the sensor activity was affected by MBP conformational changes upon maltose binding, in the presence of a saturating concentration of maltose (20 mM). The fluorescence of wtMBP complexed with either N45C or T46C sensors is sensitive to maltose, which causes the sensor to lose 5-fold activity (Fig. 3E), suggesting that the NBD pocket adopts a different configuration in the maltose bound form of MBP. Finally, we investigated how these mutations affect the interaction of MBP with the fluorophore. Using an iodide-quenching assay to determine the solvent exposure of NBD, we found that the change in solvent exposure upon complex formation with wtMBP is reduced in the presence of maltose (Fig. 3F). However for the mutation V347A, the fluorophore is further shielded from the solvent and addition of maltose has no effect. In contrast, the activity abrogating mutation V347W results in solvent exposure levels comparable to those in the absence of the MBP analyte. These results suggest that the NBD fluorophore binds to a conformationally sensitive hydrophobic pocket which is responsible for high SuCESsFul biosensor fluorescence.

We next sought to further validate the MBP structural rearrangements for NBD binding. We acquired $^{15}$N-resolved Transverse Relaxation Optimized Spectrscopy (TROSY) Heteronuclear Single Quantum Coherence (HSQC) spectra for wtMBP, with and without Off7wt and Off7(T46C)*NBD, in the absence of maltose. The chemical shifts of the unbound state matched exactly with previously published chemical shift assignments collected under identical conditions[24]. Large chemical shift changes are observed upon binding of Off7wt (Supplementary Fig. S7A) in agreement with the contact regions shown in the Off7/MBP complex crystal structure (PDB: 1SVX). The observed chemical shift perturbations for the Off7(T46C)*NBD/MBP versus the Off7wt/MBP complex are of smaller magnitude, as expected from a small molecule (Supplementary Fig. S7B). From the $^{1}$H and $^{15}$N chemical shift differences (Supplementary Fig. S7C, D), we calculated the combined weighted chemical shift perturbation and displayed the results on the Off7/MBP crystal structure (see Methods and Fig. 3G). The most strongly affected residues are found within the hypothesized NBD binding pocket, yet several distant side chains are also

affected to a lesser extent. These structural results support a model including conformational rearrangements to accommodate for NBD binding in the hydrophobic pocket.

To determine whether other DARPin-based biosensors exhibited evidence for a specific fluorophore-binding pocket on MBP, we next sought to understand the mechanism of activated fluorescence of NBD upon MBP binding when Off7 is labeled at position M114C, which is distant from the cavity identified above. Structural analysis of the complex identified 12 amino acids within interaction distance of NBD-labeled M114C (supplementary Fig. S8A, B). Alanine-scanning mutagenesis identified two residues (T193, D197) facing toward the labeling site on an α-helix as sensitive to mutation (Supplementary Fig. S8C). Next, we generated mutants of these two positions, as well as one position one turn N-terminal to the α-helix, into amino acids with a range of hydrophobic side chain sizes. We observed that mutation A190F improved the sensor by a factor of three (supplementary Fig. S8D). Furthermore, all mutations to tryptophan dramatically reduced the fluorescence activation of the sensor (Fig. S8D, E). These mutants were shown to retain binding to the DARPin by size exclusion chromatography and biolayer interferometry (supplementary Fig. S8F, S8G). We attempted to mature MBP for increased sensor activity with the YSD screen, however interestingly we did not achieve any additional enhancement in sensor fluorescence, in strong contrast to the Off7(T46C)*NBD biosensor. Furthermore, this sensor was not sensitive to maltose (Fig. 3E). These results suggest that the Off7(M114C)*NBD biosensor, with a lower $F/F_0$ than N45C and T46C, does not depend on a specific binding interaction between the fluorophore and a binding pocket on MBP, perhaps relying on a more nonspecific solvent shielding mechanism for fluorescence enhancement.

## Rigid scaffolds lower background fluorescence

Two different types of SuCESsFul biosensors are apparent among those described so far: the first, exemplified by Off7(N45C)*NBD and Off7(T46C)*NBD, is defined by the apparent presence of a specific fluorophore binding pocket in the analyte, yielding strong fluorescence enhancements. The second, and far more common class, exemplified by Off7(M114C)*NBD, shows increase in fluorescence due to more nonspecific shielding, achieving a $F/F_0$ ratio greater than one, primarily because the background fluorescence intensity of the unbound biosensor is low (Fig. 4A). We hypothesized that high background fluorescence may arise from an intramolecular interaction between the conjugated fluorophore and the binding protein. In order to investigate this interaction, we measured the background fluorescence (i.e. in the absence of the analyte) of NBD labeled Off7 and Fn3 with and without a fusion partner. We found that fusing Off7 to a Sumo coexpression tag resulted in a shift of the background fluorescence toward shorter wavelengths (i.e. to a more activated state) (Fig. 4B), suggesting that interactions with the fusion partner can raise the background fluorescence. When labeled with NBD, we found that Fn3s show a significantly lower emission wavelength than the Off7-based mutants (Fig. 4B), possibly resulting from the flexibility of the Fn3 loops, which may increase the potential for intramolecular interaction. In light of these observations, we hypothesized that undesirable fluorophore pre-activation might be attenuated by employing a small and rigid protein scaffold. We considered the scaffold Sso7d as a candidate; Sso7d is a small (~7 kDa) protein consisting of

an incomplete β-barrel with five β-strands and a C-terminal α-helix. Recently, our group developed a yeast library based on this scaffold, using three β-strands as the binding interface. We hypothesized that the rigid conformation of the β-strands would reduce the likelihood of fluorophore interactions with the scaffold, thereby reducing unwanted background fluorescence. The Sso7d scaffold homolog Sac7d has recently been demonstrated to be applicable to SuCESsFul biosensors[6]. We used a murine serum albumin binder, clone M11.1.3, and labeled it at seven sites of the engineered planar binding surface, as well as three sites in the loops connecting the strands, the C-terminus, and one near the N-terminus (supplementary Fig. S9A). When labeled with NBD, we observed that the maximum emission wavelength for unbound biosensors was significantly longer than for Off7 or Fn3, directly demonstrating reduced background activation with this scaffold. Furthermore, the fluorescence intensity was also lower (supplementary Fig. S9B). These promising results were further validated using another Sso7d mutant M18.2.5 (supplementary Fig. S9A–B).

### Combination of rigid scaffold with a specific fluorophore binding pocket yields largest dynamic range

Having established Sso7d as a promising scaffold for SuCESsFul biosensors given the lower fluorescence intensity of unbound conjugates, we sought to validate the hypothesis that specific fluorophore binding pockets enhance fluorescence signals. To do so, we screened several analytes for the presence of an NBD binding pocket. The fluorescence of NBD is unchanged upon addition of 10 μM lysozyme or MBP. However, in the presence of 10 μM mouse serum albumin, the maximum emission is shifted to shorter wavelengths and the intensity increases 8-fold (supplementary Fig. S9C), strongly suggesting that NBD binds MSA. Based on these results, we chose the MSA-binding clone M11.1.3; when labeled with NBD, we found that positions I23C, W25C and G26C, showed greater than 50-fold increases in fluorescence upon addition of 10 μM MSA (Fig. 4C). To validate this cluster, we used another MSA binding clone: in agreement with the results with M11.1.3, labeling M18.2.5 at positions 23, 25 and 26 resulted in the largest $F/F_0$ ratio (supplementary Fig. S9D). We measured the $K_D$ for NBD/MSA interaction to be 19.7 μM, and found that M18.2.5(L25C)*NBD had a 30-fold tighter equilibrium binding constant, $K_D$ = 0.38 μM (Fig. 4D). Importantly, titration experiments demonstrated that the affinities of M11.1.3(W25C)*NBD, M11.1.3(G26C)*NBD and M18.2.5(L25C)*NBD were at least 10-fold higher, respectively, when compared to free NBD. Furthermore, addition of non-labeled M11.1.3 or M18.2.5 binders blocked biosensor activity of the labeled binders, but not of free NBD, confirming that binding of the Sso7d-based proteins to MSA is necessary for the biosensor activity and that the binding mode of those Sso7d-NBD fusions is different from free NBD. (Supplementary Fig. S9E).

## Discussion

Altogether, we investigated three types of scaffolds, eight analytes, and ten fluorophores in 448 combinations as components of a SuCESsFul biosensor system, which is to our knowledge, the largest such dataset available to date. Previous studies have been mostly limited to one class of fluorophore or one scaffold and have not elucidated *general* design

principles. Excluding the Sso7d results, we obtained an overall, unbiased success rate similar to what has been reported previously in the literature (Fig. 1C). Surprised by the rarity of useful sensors produced by the consensus design approach, we explored the physical basis for a successful example. The complexes Off7(N45C)*NBD/MBP and Off7(T46C)*NBD/MBP showed the brightest signal intensity, and the greatest $F/F_0$ ratio previously reported. Also, the emission wavelength of NBD was strongly blue-shifted upon complex formation, indicating a reduced polarity in the binding pocket of the fluorophore[25].

Several factors can be responsible for the fluorescence blue shift and increased intensity upon complex formation of NBD. The important feature characterizing the fluorescence properties of NBD is the charge transfer occurring between the amino group (electron donor) and the nitro group (electron acceptor). Excitation by a photon of the appropriate energy accentuates the dipole between the acceptor and donor groups. Stabilization of the dipole will reduce the energy of the excited state and thus, the energy of the released photon[26]. Stabilization can arise from multiple factors. 1) Polar solvents stabilize the charged configuration by dipole-dipole interactions, which lowers the energy of the excited state and increases the non radiative decay ($k_{nr}$)[25]. 2) H-bonding between the solvent and an oxygen of the nitro group, which would reinforce the electronic attraction of the acceptor[25]. 3) Dynamic relaxation with internal twisting of the dimethylamino group, coupled with an electron transfer. Twisted intramolecular charge transfer (TICT) is the result of an intramolecular rotation where the acceptor and donor are orbitally decoupled. TICT states are non luminescent[27]. Both static approaches, by rigidifying the amino group via covalent bonds, and dynamic approaches, by increasing the volume of the groups attached to the nitrogen, have supported this theory[28]. Decrease in the $k_{nr}$ with increased solvent viscosity and lower temperatures also support the involvement of a TICT dependent fluorescence[25]. Hence, our data supports the hypothesis of a specific interaction of NBD with a hydrophobic cavity – blue-shifted emission shift – which restricts the motion of the fluorophore and prevents it from accessing a TICT state, and thus exhibits a greater quantum yield.

We have further confirmed the existence of this binding pocket using a solution NMR chemical shift perturbation and by identifying sensor enhancing mutations using a yeast surface display screen (Fig. 3), evolving MBP to become a better analyte for the Off7(T46C)*NBD sensor. We found that the majority of mutations accumulated within the putative NBD binding pocket. We also observed that mutations along the α-helix mutated between amino acids 150–158, constituting part of the putative NBD binding pocket, were intolerant to mutations, suggesting that these residues are critical for the interaction with NBD. Furthermore, Glu 153, Tyr 155 and Tyr 156 make direct van der Waals contact with maltose[29] and may be important for the structural integrity of the cavity. Szent-Gyorgyi *et al* have used yeast surface display to isolate single chain variable fragments (scFv) binding to and activating the fluorescence of malachite green[30] in a mechanism also involving TICT[27,31]. Thus, the fluorescence of both NBD and Malachite Green can be strongly activated upon the presence of a specific binding pocket in a protein.

We also found that maltose acts as an allosteric regulator of sensor activity (Fig. 3E). The binding site for maltose is located at the cleft between the two domains[29]. Upon maltose binding by wtMBP, the activity of the Off7(T46C)*NBD sensor is affect by a 5-fold factor.

Through our yeast surface display analyte maturation screen, we identified a multitude of mutations located in domain I or at the hinge between domains I and II. These mutations are not involved in direct contacts with maltose[29], yet they may affect MBP conformation or dynamics. It is known that in the analyte-free form, MBP exists 95% in an open-state, and 5% in a partially closed state[32]. The transition between major (open) and minor forms of apo MBP involves a hinge rotation of 33 ± 7° in comparison with 35° between open and closed holo MBP. However, the apo minor and closed holo states of MBP are distinct and related by a domain reorientation of 18° that is accompanied by a 6 A translation[32] . The mutations we observed may affect this equilibrium away from the partially closed state, or a distinct conformation that favors interaction of NBD with its pocket. This is supported by the observation of activity enhancing mutations and that the NBD interaction with the cavity is impeded in the maltose-bound form of MBP. Finally, NBD has been employed as a maltose sensor when conjugated to MBP, and TICT has been hypothesized as the mechanism for the slight 1.8-fold increase in fluorescence[33].

In this study, we did not observe dramatic fluorescence increases with any other of the environment sensitive fluorophores tested. Yet, these have also been shown to exhibit strong solvent-dependent changes in fluorescence emission properties. In particular, the naphthalimide derivative 4-DMN has demonstrated greater fluorescence increase than NBD or Badan in the context of the M13 peptide and Calmodulin interaction[34]. Furthermore, while we have not investigated merocyanine derivatives in this study, they represent also an interesting category of solvatochromic fluorophores and have been implemented for biosensors design with success[35,36]. As we have demonstrated in this manuscript, the nature of the fluorophore, analyte and scaffold interaction is critical and difficult to predict. Therefore, we encourage researchers designing this class of sensors and seeking very high levels of fluorescence activation to try fluorophores with distinct chemical structures.

While we identified the specific binding pocket as a mechanism for very large activation of NBD, fortunately, the presence of a binding pocket is not an absolute requirement for useful sensor activity. M114C undergoes a five-fold increase in fluorescence with a minor blue-shift (2 nm) without a hydrophobic pocket; the polarity of the environment of NBD is unaffected. The epitope analysis did not identify the presence of an NBD-binding pocket on MBP for this biosensor and thus we speculate that its fluorescence intensity increase is mostly due to motional restriction, leading to an increase in fluorescence intensity by increasing the energy of the TICT state.

Our data highlight the importance of the fluorophore interactions with the analyte for fluorescence activation. The nature of these interactions are also important, as exemplified in the literature where NBD-dependent binders were previously selected and yet showed little optical response to analyte[37]. The involvement of binding pockets has been exploited previously with NBD derivatives binding to trypsinogen and the 50S ribosomal subunit as well as Nile Red binding to several other large proteins[38,39]. Binding sites for small molecules are not uncommon and there are strategies to identify them[40–43]. However, screening for binders whose epitopes lie sufficiently near the fluorophore binding pocket further complicate the process, and thus we sought to establish a more generalizable approach to designing SuCESsFul biosensors.

Next, we analyzed the fluorescence intensity and emission wavelength of three Off7 sensors in the presence of all MBP mutants designed in this study (Fig. 4A). At the far right, we can navigate through increases in fluorescence without changes in the emission wavelength, resulting from shielding of the fluorophore by MBP: the sensor Off7(M114C)*NBD relies on this mechanism. In the middle range, there is a stronger relationship between emission wavelength and intensity, resulting from an interaction with a fluorophore binding pocket: sensors Off7(N45C)*NBD and Off7(T46C)*NBD rely on this mechanism.

A general solution to developing SuCESsFul biosensors is to start with very low fluorescence activation in the unbound state. Prevention of intramolecular interactions in the unbound biosensor plays a major, yet previously unappreciated, role in sensor performance. The interactions between fluorophores and scaffold are difficult to predict and we did not identify trends relating emission wavelengths and properties of surrounding amino acid side chains amongst the various constructs investigated. The presence of a fusion partner, such as SUMO, to simplify expression led to higher background fluorescence. It is noteworthy that peptide-based SuCESsFul biosensors have been found to exhibit both very low background fluorescence and high dynamic range, most likely due to the absence of strong intramolecular fluorophore interactions in the unbound state[44–46].

We further hypothesized that structural rigidity of DARPin over Fn3 scaffolds may be a contributing factor to the success of this Off7/MBP system. In order to test this hypothesis, we used the hyperthermostable Sso7d scaffold whose binding paratope is comprises three beta-strands. For two Sso7d derived mutants (M11.1.3 and M18.2.5) labeled at various positions on and around the engineered binding epitope, we observed that the fluorescence emission maxima was significantly longer than that of Fn3 or Off7, resembling more the emission of the non-conjugated fluorophore (Fig. 4B). The fluorescence intensity for these constructs was also lower (Fig. S5C). Our results support the hypothesis that local conformational rigidity can reduce fluorophore pre-activation due to intramolecular interactions. Based on the low background fluorescence of NBD labeled Sso7d, we developed sensors for MSA as a proof-of-concept, and obtained up to a 100-fold increase in fluorescence on analyte binding. This represents the greatest fold increase in fluorescence yet reported for a protein-protein SuCESsFul biosensor. When evaluating the best sensor from a DARPin, Fn3 and Sso7d scaffold (Fig 4E), it stands out that the success of Sso7d as a scaffold for SuCESsFul biosensor can be attributed to its reduced background fluorescence.

We have demonstrated that combining low background intensity with an enhanced activated state, a SuCESsFul biosensor can be built with greater than 100-fold increase in fluorescence upon analyte binding. SuCESsFul biosensor design falls within three broad categories (Fig. 4F), two of which can lead to larger $F/F_0$ ratios. In one scenario, the successful design is driven by achieving very strong fluorescence intensity mediated by a fluorophore-specific binding pocket, as we have demonstrated for Off7(T46C)*NBD. A panel of fluorophores could be screened against an analyte of interest to identify the presence of a binding pocket through methods such as fluorescence, NMR or computational docking. Once a fluorophore is selected, the development of several binders is necessary to target the correct epitope. This medicinal-chemistry like fragment-based discovery approach would be intensive in terms of time and resources. On the other hand, one can build sensors with more modest $F/F_0$ ratios

(~10-fold for NBD), drawing on the second scenario of lower unbound fluorescence rather than dramatically higher bound fluorescence. The use of rigid scaffolds like Sso7d with lower background can significantly increase the odds of design success. Combination of both scenarios yields, as we have demonstrated, sensors with up to 100-fold increase in fluorescence. Beyond protein-protein interactions, these guidelines could help in the design of any improved sensor using solvatochromic fluorophores.

## Supplementary Material

Refer to Web version on PubMed Central for supplementary material.

## Acknowledgments

This work was supported by a grant from the National Science Foundation (MCB-115803), NIH/NCI Integrated Cancer Biology Program U54CA112967 and NIH R01 EB 010246. B.S.M. is a NIH pre-doctoral trainee (GM071339). We thank the Koch Institute Flow Cytometry Core facility and Biopolymers Core facility for FACS experiments and sequencing, respectively. We are also grateful to Dr. Nicole Yang for comments on the manuscript.

## Abbreviations

| | |
|---|---|
| **Fn3** | $10^{th}$ type 3 domain of human fibronectin |
| **DARPin** | designed ankyrin repeat protein |
| **NBD** | nitrobenz-2-Oxa-1,3-Diazole |
| **MBP** | maltose binding protein |
| **Sso7d** | small DNA binding domain derived from *Sulfolobus solfataricus* |
| **MSA** | mouse serum albumin |
| **TICT** | twisted internal charge transfer |

## References

1. Zadran S, et al. Fluorescence resonance energy transfer (FRET)-based biosensors: visualizing cellular dynamics and bioenergetics. Appl Microbiol Biotechnol. 2012; 96:895–902. [PubMed: 23053099]
2. Burr M, Koshland DE. Use of ‘Reporter Groups’ in Structure-Function Studies of Proteins. Proc Natl Acad Sci. 1964; 52:1017–1024. [PubMed: 14224379]
3. Renard M, et al. Knowledge-based design of reagentless fluorescent biosensors from recombinant antibodies. J Mol Biol. 2002; 318:429–42. [PubMed: 12051849]
4. Brient-Litzler E, Pluckthun A, Bedouelle H. Knowledge-based design of reagentless fluorescent biosensors from a designed ankyrin repeat protein. Protein Eng Des Sel. 2010; 23:229–41. [PubMed: 19945965]
5. Gulyani A, et al. A biosensor generated via high-throughput screening quantifies cell edge Src dynamics. Nat Chem Biol. 2011; 7:437–44. [PubMed: 21666688]
6. Miranda FF, Brient-Litzler E, Zidane N, Pecorari F, Bedouelle H. Reagentless fluorescent biosensors from artificial families of antigen binding proteins. Biosens Bioelectron. 2011; 26:4184–90. [PubMed: 21565483]
7. Kummer L, et al. Knowledge-Based Design of a Biosensor to Quantify Localized ERK Activation in Living Cells. Chem Biol. 2013; 20:847–56. [PubMed: 23790495]

8. Renard M, Belkadi L, Bedouelle H. Deriving Topological Constraints from Functional Data for the Design of Reagentless Fluorescent Immunosensors. J Mol Biol. 2003; 326:167–175. [PubMed: 12547199]

9. Chao G, et al. Isolating and engineering human antibodies using yeast surface display. Nat Protoc. 2006; 1:755–68. [PubMed: 17406305]

10. Hanes J, Pluckthun a. In vitro selection and evolution of functional proteins by using ribosome display. Proc Natl Acad Sci U S A. 1997; 94:4937–42. [PubMed: 9144168]

11. Roberts RW, Szostak JW. RNA-peptide fusions for the in vitro selection of peptides and proteins. Proc Natl Acad Sci U S A. 1997; 94:12297–12302. [PubMed: 9356443]

12. Clackson T, Hoogenboom H, Griffiths A, Winter G. Making antibody fragments using phage display libraries. Nature. 1991; 352:624–628. [PubMed: 1907718]

13. Koide, a; Bailey, CW.; Huang, X.; Koide, S. The fibronectin type III domain as a scaffold for novel binding proteins. J Mol Biol. 1998; 284:1141–51. [PubMed: 9837732]

14. Binz HK, et al. High-affinity binders selected from designed ankyrin repeat protein libraries. Nat Biotechnol. 2004; 22:575–82. [PubMed: 15097997]

15. Liao X, Rabideau AE, Pentelute BL. Delivery of Antibody Mimics into Mammalian Cells via Anthrax Toxin Protective Antigen. Chembiochem. 2014; 15:2458–2466. [PubMed: 25250705]

16. De Picciotto S, Imperiali B, Griffith LG, Wittrup KD. Equilibrium and dynamic design principles for binding molecules engineered for reagentless biosensors. Anal Biochem. 2014; 460:9–15. [PubMed: 24814226]

17. Spicer CD, Davis BG. Selective chemical protein modification. Nat Commun. 2014; 5:1–14.

18. Rashidian M, Dozier JK, Distefano MD. Enzymatic Labeling of Proteins: Techniques and Approaches. Bioconjug Chem. 2013; 24:1277–1294. [PubMed: 23837885]

19. Hackel BJ, Wittrup KD. The full amino acid repertoire is superior to serine/tyrosine for selection of high affinity immunoglobulin G binders from the fibronectin scaffold. Protein Eng Des Sel. 2010; 23:211–9. [PubMed: 20067921]

20. Chen TF, de Picciotto S, Hackel BJ, Wittrup KD. Elsevier Inc. Methods in enzymology. 2013; 523:303–26. [PubMed: 23422436]

21. Gilbreth RN, Esaki K, Koide A, Sidhu SS, Koide S. A dominant conformational role for amino acid diversity in minimalist protein-protein interfaces. J Mol Biol. 2008; 381:407–18. [PubMed: 18602117]

22. Koide A, Wojcik J, Gilbreth RN, Hoey RJ, Koide S. Teaching an old scaffold new tricks: monobodies constructed using alternative surfaces of the FN3 scaffold. J Mol Biol. 2012; 415:393–405. [PubMed: 22198408]

23. Hackel BJ, Kapila A, Wittrup KD. Picomolar affinity fibronectin domains engineered utilizing loop length diversity, recursive mutagenesis, and loop shuffling. J Mol Biol. 2008; 381:1238–52. [PubMed: 18602401]

24. Evenas J, et al. Ligand-induced structural changes to maltodextrin-binding protein as studied by solution NMR spectroscopy. J Mol Biol. 2001; 309:961–974. [PubMed: 11399072]

25. Fery-forgues S, Fayet J, Lopez A. Drastic changes in the fluorescence properties of NBD probes with the polarity of the medium : involvement of a TICT state ? J Photochem Photobiol A Chem. 1993; 70:229–243.

26. Loving GS, Sainlos M, Imperiali B. Monitoring protein interactions and dynamics with solvatochromic fluorophores. Trends Biotechnol. 2010; 28:73–83. [PubMed: 19962774]

27. Rettig W. Charge separation in excited-states of decoupled systems - TICT compounds and implications regarding the development of new laser-dyes and the primary processes of vision and photosynthesis. Angew Chem Int Ed Engl. 1986; 25:969–986.

28. Rettig WGR. Dependence of Intramolecular Rotation in p-Cyano-N,N-dialkylanilines on the Twist Angle. A Fluorescence, UV Absoprtion, and Photoelectron Spectroscopic Study. J Phys Chem. 1985; 89:4676–4680.

29. Spurlino JC, Lu GY, Quiocho FA. The 2.3-A resolution structure of the maltose- or maltodextrin-binding protein, a primary receptor of bacterial active transport and chemotaxis. J Biol Chem. 1991; 266:5202–19. [PubMed: 2002054]

30. Szent-Gyorgyi C, et al. Fluorogen-activating single-chain antibodies for imaging cell surface proteins. Nat Biotechnol. 2008; 26:235–40. [PubMed: 18157118]
31. Grimm JB, et al. A general method to improve fluorophores for live-cell and single-molecule microscopy. Nat Methods. 2015:12.
32. Tang C, Schwieters CD, Clore GM. Open-to-closed transition in apo maltose-binding protein observed by paramagnetic NMR. Nature. 2007; 449:1078–1082. [PubMed: 17960247]
33. Gilardi G, Mei G, Rosato N, Agro aF, Cass aE. Spectroscopic properties of an engineered maltose binding protein. Protein Eng. 1997; 10:479–486. [PubMed: 9215565]
34. Loving G, Imperiali B. A versatile amino acid analogue of the solvatochromic fluorophore 4-N,N-dimethylamino-1,8-naphthalimide: a powerful tool for the study of dynamic protein interactions. J Am Chem Soc. 2008; 130:13630–8. [PubMed: 18808123]
35. Nalbant P, Hodgson L, Kraynov V, Toutchkine A, Hahn KM. Activation of endogenous Cdc42 visualized in living cells. Science. 2004; 305:1615–9. [PubMed: 15361624]
36. Macnevin CJ, et al. Environment-Sensing Merocyanine Dyes for Live Cell Imaging Applications. Bioconjug Chem. 2013; doi: 10.1021/bc3005073
37. Jespers L, Bonnert TP, Winter G. Selection of optical biosensors from chemisynthetic antibody libraries. Protein Eng Des Sel. 2004; 17:709–713. [PubMed: 15537669]
38. Kenner RA, Aboderin AA. A new fluorescent probe for protein and nucleoprotein conformation. Binding of 7-(p-methoxybenzylamino)-4-nitrobenzoxadiazole to bovine trypsinogen and bacterial ribosomes. Biochemistry. 1971; 10:4433–40. [PubMed: 4946923]
39. Sackett DL, Wolff J. Nile red as a polarity-sensitive fluorescent probe of hydrophobic protein surfaces. Anal Biochem. 1987; 167:228–234. [PubMed: 3442318]
40. Luchini A, Espina V, Liotta LA. Protein painting reveals solvent-excluded drug targets hidden within native protein-protein interfaces. Nat Commun. 2014; 5:4413. [PubMed: 25048602]
41. Taylor RD, Jewsbury PJ, Essex JW. A review of protein-small molecule docking methods. J Comput Aided Mol Des. 2002; 16:151–166. [PubMed: 12363215]
42. Shuker SB, Hajduk PJ, Meadows RP, Fesik SW. Discovering high-affinity ligands for proteins: SAR by NMR. Science. 1996; 274:1531–1534. [PubMed: 8929414]
43. Villar, Ea, et al. How proteins bind macrocycles. Nat Chem Biol. 2014; 10:1–10.
44. Goguen BN, Loving GS, Imperiali B. Development of a fluorogenic sensor for activated Cdc42. Bioorg Med Chem Lett. 2011; 21:2–5.
45. Loving G, Imperiali B. Thiol-reactive derivatives of the solvatochromic 4-N,N-dimethylamino-1,8-naphthalimide fluorophore: a highly sensitive toolset for the detection of biomolecular interactions. Bioconjug Chem. 2009; 20:2133–41. [PubMed: 19821578]
46. Venkatraman P, et al. Fluorogenic probes for monitoring peptide binding to class II MHC proteins in living cells. Nat Chem Biol. 2007; 3:222–8. [PubMed: 17351628]
47. Krueger AT, Kroll C, Sanchez E, Griffith LG, Imperiali B. Tailoring Chimeric Ligands for Studying and Biasing ErbB Receptor Family Interactions. Angew Chem Int Ed Engl. 2014; :1–6. DOI: 10.1002/anie.201307869
48. Sainlos M, Imperiali B. Tools for investigating peptide-protein interactions: peptide incorporation of environment-sensitive fluorophores through SPPS-based ‘building block’ approach. Nat Protoc. 2007; 2:3210–3218. [PubMed: 18079721]
49. Watt RM, Voss EW. Mechanism of quenching of fluorescein by anti-fluorescein IgG antibodies. Immunochemistry. 1977; 14:533–51. [PubMed: 303233]
50. Nucci NV, et al. Optimization of NMR spectroscopy of encapsulated proteins dissolved in low viscosity fluids. J Biomol NMR. 2011; 50:421–430. [PubMed: 21748265]
51. Gardner KH, Zhang X, Gehring K, Kay LE. Solution NMR studies of a 42 kDa E. coli maltose binding protein/b cyclodextrin complex: chemical shift assignments and analysis. J Am Chem Soc. 1998; 120:11738–11748.
52. Hyberts SG, Milbradt AG, Wagner AB, Arthanari H, Wagner G. Application of iterative soft thresholding for fast reconstruction of NMR data non-uniformly sampled with multidimensional Poisson Gap scheduling. J Biomol NMR. 2012; 52:315–327. [PubMed: 22331404]

53. Hyberts SG, Takeuchi K, Wagner G. Poisson-gap sampling and forward maximum entropy reconstruction for enhancing the resolution and sensitivity of protein NMR data. J Am Chem Soc. 2010; 132:2145–2147. [PubMed: 20121194]

54. Salzmann M, Pervushin K, Wider G, Senn H, Wuthrich K. TROSY in triple-resonance experiments: new perspectives for sequential NMR assignment of large proteins. Proc Natl Acad Sci U S A. 1998; 95:13585–13590. [PubMed: 9811843]

55. Salzmann M, Wider G, Pervushin K, Senn H, Wuthrich K. TROSY-type triple resonance experiments for sequential NMR assignment of large proteins. J Am Chem Soc. 1999; 121:844–848.

56. Delaglio F, et al. NMRPipe: A multidimensional spectral processing system based on UNIX pipes. J Biomol NMR. 1995; 6:277–293. [PubMed: 8520220]

57. Goddard, T.; Kneller, D. SPARKY. University of California; San Francisco: 2014.

58. Schrodinger LLC. PyMOL.

59. Mata-Fink J, et al. Rapid Conformational Epitope Mapping of anti-gp120 Antibodies with a Designed Mutant Panel Displayed on Yeast. J Mol Biol. 2012; 425:444–456. [PubMed: 23159556]

## Highlights

- SuCESsFul biosensors report protein interactions via environment sensitive dyes.
- We observed that the current design principles are insufficient.
- Fluorophore binding pockets are required for strong fluorescence activation.
- Scaffold/fluorophore interactions can raise background fluorescence.
- Applying our new design criteria, we engineered the most responsive sensor to date.

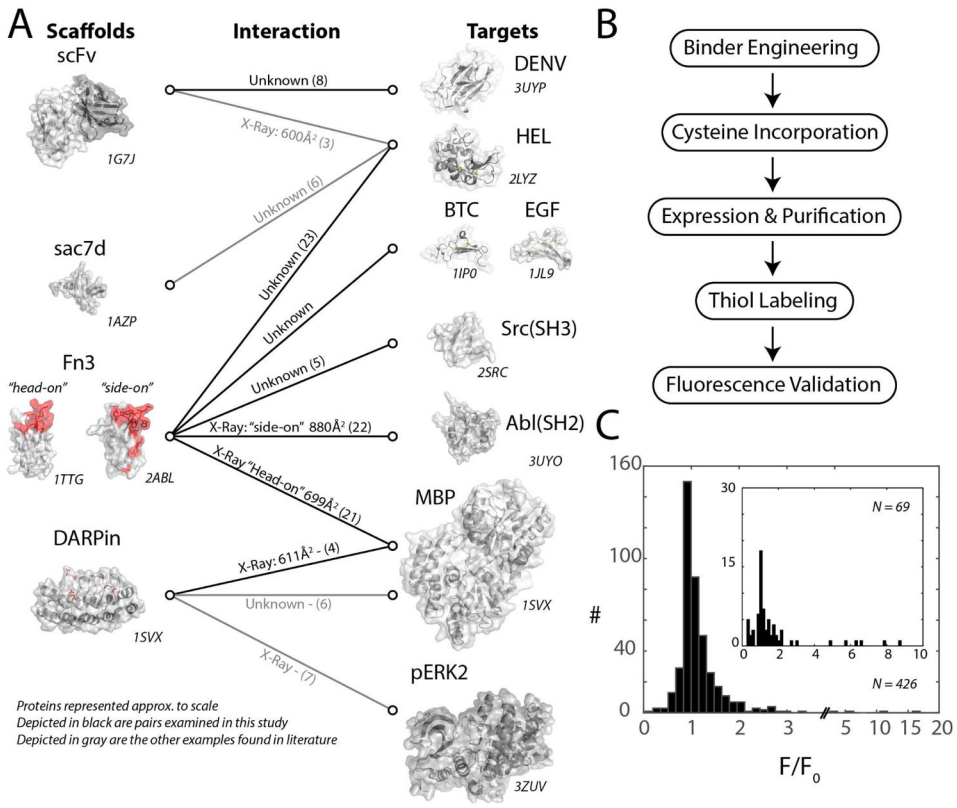


**Figure 1.**

Reagentless biosensor workflow and overview. A) Overview of reported reagentless biosensors built from a protein scaffold recognizing another protein. On the left side the various protein scaffolds that have been used and coupled with an environment-sensitive dye are listed. On the right side the target proteins are shown. Dark arrows represent pairs evaluated in this study. The connecting lines indicate the information about the nature of the interaction as well as the reference citation. B) Reagentless biosensor engineering is a five-step process. First, a binder must be engineered with desired specificity and affinity. Second, a chemical moiety for site-specific labeling must be incorporated. This is typically achieved by directed mutagenesis for a cysteine at the desired location. Next, the protein construct is expressed, purified and labeled with a thiol reactive derivative of the fluorescent dye. Finally the construct is evaluated for its fluorescence characteristic in the absence and presence of its target. C) Histogram of the dynamic range of sensors to their target reported as $F/F_0$, the fluorescence intensity ratio between the conditions in presence versus in absence of the target protein. The histogram showed in the inlet is from previously published results[1–4].

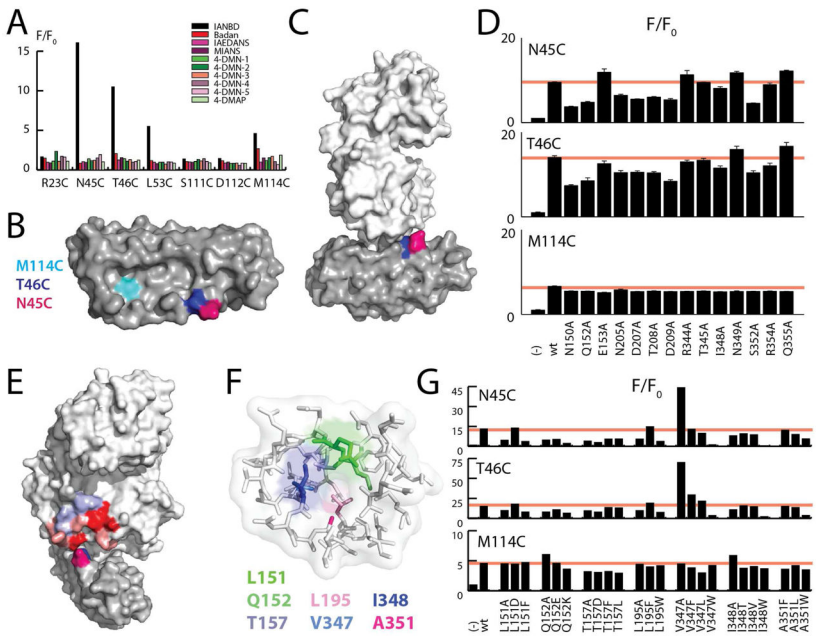


**Figure 2.**

Mapping the interaction between NBD and MBP in the Off7(N45C)*NBD and Off7(T46C)*NBD sensors. A) Increase in fluorescence signal when adding MBP to Off7 mutants labeled with 10 different fluorophores at 7 positions. B) Top view of the Off7 protein (PBD: 1SVX). C) Side view of the Off7/MBP complex (PDB: 1SVX). D) $F/F_0$ ratios of 3 Off7*NBD sensors with wtMBP and mutants with a single alanine mutation. E) Effects from alanine scanning are plotted against the Off7/MBP structure, red indicates reduced activity, blue increased activity. Deleterious mutations are surrounding a cavity in MBP. F) Residues mutated in the cavity analysis. G) $F/F_0$ ratios for three Off7*NBD sensors with MBP cavity mutants.

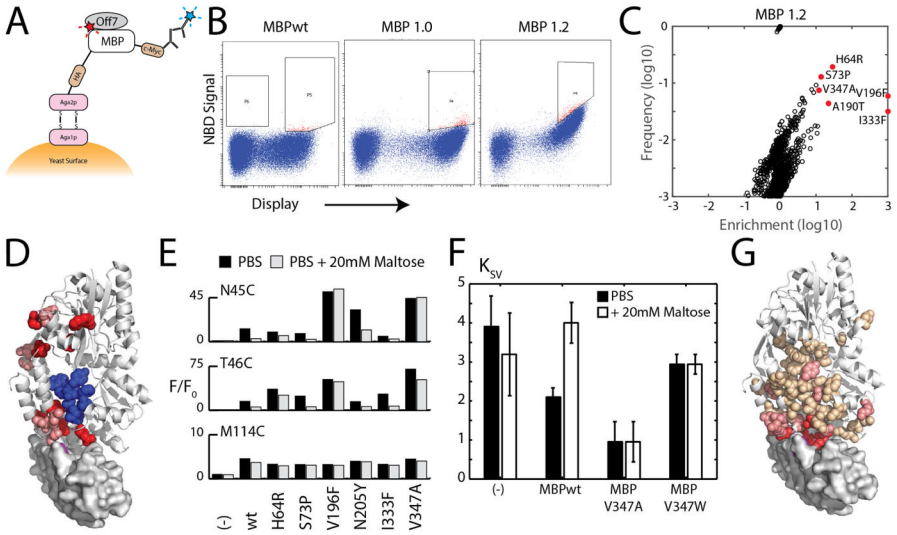


**Figure 3.**

Off7(T46C)*NBD Sensor is regulated by MBP conformation. A) Graphical representation of experimental set-up. B) FACS plots showing the improvement of NBD signal produced by MBP mutant displaying yeasts over two selection rounds. C) Enrichment versus frequency plot for the whole gene error prone PCR library. D) Graphical representation of enrichment onto Off7/MBP structure combined from all four libraries. Red and blue indicate positive and negative enrichment respectively. E) $F/F_0$ ratios for the YSD isolated mutants in the absence or presence of maltose. Mutations H64R, V196F and V347A greatly stabilized the activity of the sensor in the presence of maltose. F) Iodide quenching assay, reporting the Stern-Vollmer constant for wild-type MBP, the most strongly activating mutation V347A, and the most deteriorating mutation V347W. G) Weighted combined nitrogen and proton chemical shift perturbations (CSP) are highlighted on the Off7/MBP complex. CSP between 0.025 and 0.05 are shown in beige, between 0.05 and 0.1 in salmon, and CSP > 0.1 in red.

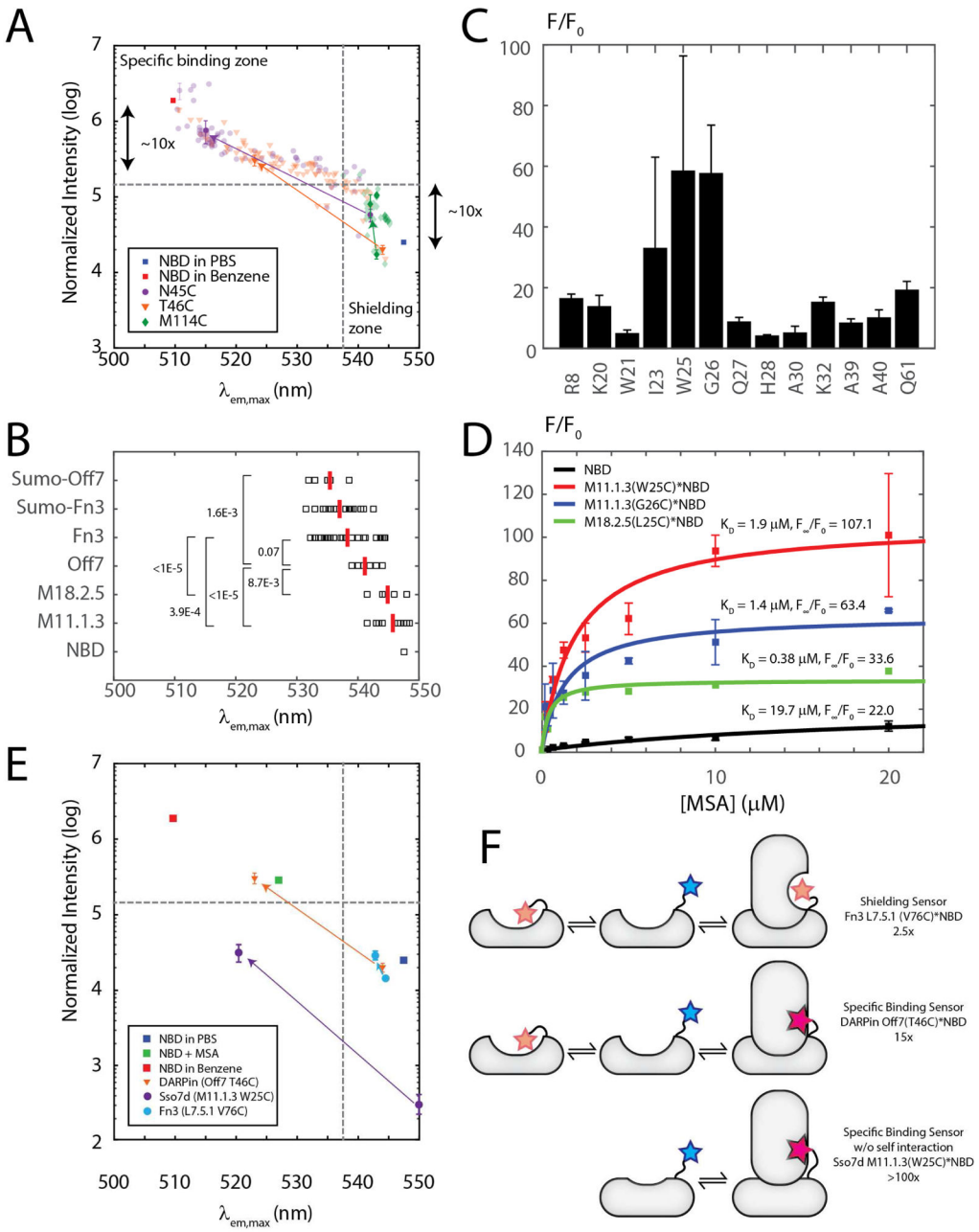


**Figure 4.**

The balance between scaffold rigidity and specific binding pockets. A) Maximum emission wavelength versus signal intensity plotted for the three Off7 sensors in complex with all MBP mutants evaluated in this study. In addition, free NBD in PBS and benzene is depicted. B) Maximum emission wavelength of NBD labeled scaffolds in the absence of antigen. C) $F/F_0$ ratio for M11.1.3*NBD conjugates. D) Titrations of NBD and NBD labeled constructs with MSA. E) Maximum emission wavelength vs intensity for the best Fn3, DARPin, and Sso7d sensors. F) Mechanistic drawing of the three types of reagentless biosensors. The top one describes a sensors that suffers from pre-activation and the fluorophore undergoes

shielding upon binding, yielding a small $F/F_0$ ratio. The middle one describes a sensor that may have some pre-activation but that alleviates this drawback by having a strong fluorescence enhancement due to a fluorophore binding pocket. The bottom scenario describes a sensor that possesses both ideal properties: little self-interaction and specific binding pocket interaction on the analyte.